Electrochemical Studies on $LaNi_{5-x}Sn_x$ Metal Hydride Alloys

B. V. Ratnakumar

Electrochemical Technologies Group, Jet Propulsion Laboratory

4800, Oak Grow Dr., Pasadena, California 91109

and

C. Witham, R.C. Bowman, Jr., A. Hightower, and B. Fultz

Division of Engineering and Applied Science

California Institute of Technology, Pasadena, California 91125

ABSTRACT

We present electrochemical studies on $LaNi_{5-x}Sn_x$ with $0 \leq x \leq 0.5$. We measured the effect of the Sn substituent on the kinetics of charge transfer and diffusion during hydrogen absorption and desorption, and the cyclic lifetimes of $LaNi_{5-x}Sn_x$ electrodes in 250 mAh laboratory test cells. We report beneficial effects of making small substitutions of Sn for Ni in $LaNi_5$ on the performance of the MH alloy anode in terms of cycle life, capacity and kinetics. We discuss optimizing the Sn concentration $LaNi_{5-x}Sn_x$ alloys for negative electrodes in alkaline rechargeable secondary cells.

IN'1'RODIJCJ'1ON

The usc of metal hydrides as negative electrodes in alkaline rechargeable cells is becoming inci casingly popular, owing to advantages of the metal hydrides over conventional anode materials (such as Zn, Cd) in specific energy, cyclic lifetime and environmental compatibility. The similarities in the cell voltage, pressure characteristics and charge control methods of the Ni-MH cells to the commonly used Ni-Cd cell suggest that Ni-M} 1 cells may take over a good fraction of the rechargeable battery market for consumer electronics in the next few years.

Two classes of metal hydrides alloys currently being developed are those based on rare earth metals (AB_5)[1,2] and on early transition metals (AB_2)[3]. Although AB_2 alloys are reported to exhibit higher specific energy than the AB_5 alloys, state-of-the-art commercial Ni-MH cells predominantly use AB_5 alloys The AB_5 alloys arc based on $LaNi_5$ with various substituents for La and Ni. The systematic effects of these alloy modifications, and the reasons for these effects, are active topics of research. An important goal of an alloy modification is to increase the lifetime of the MH electrode under charge-discharge cycling. It has been found that the cyclic lifetime is affected by the alloy modifications, but it is not clear why. Improved cyclic lifetimes with Co substitutions have been attributed to a reduced volume change upon hydrogen absorption and resorption.' Sakai,

et al.[4] studied various ternary substitutions for Ni in $LaNi_5$, and reported that the cyclic lifetime improves with the ternary substituents studied in the order Mn < Ni < Cu < Cr < Al < Co. It has also been suggested that the substitution of the rare earth metal with Ti[5], Zr[6] or other lanthanides such as Nd[1] and Ce[7] may promote the formation of a protective surface film and enhance the cyclic lifetime This is auspicious for the use of relatively inexpensive misch metal, Mm (a naturally occurring mixture of rare earth metals La, Ce, Pr and Nd) for La in alloy formulations such as $(Mm)(Ni\text{-}Co\text{-}Mn\text{-}Al)_5$.[8,9]

The beneficial effect of the substituents for either La or Ni is often accompanied by an undesirable decrease in the hydrogen absorption capacity, long activation and slow kinetics of hydrogen absorption and resorption. In our recent communications,[10,11] we described the advantages associated with using Sn as a ternary substituent. The addition of small amounts (3.3 ate%) of Sn improves the cycle life and the kinetics of absorption and resorption, with a marginal reduction in the specific capacity. The specific capacity of $LaNi_{4.8}Sn_{0.2}$ is about 300 mAh/g and is retained well during charge-discharge cycling. The benefits of alloying with Sn have also been realized in multi-component alloys.[12] In this paper, we present results from further studies on the Sri-modified $LaNi_5$ alloys of differing Sn concentrations. These studies were aimed at identifying the effect of the Sn additive on electrochemical characteristics of the metal hydride all oys, including the

kinetics of charge transfer and diffusion during the hydriding process, and cyclic lifetimes in 250 mAh laboratory test cells.

EXPERIMENTAL

The $LaNi_{5-x}Sn_x$ alloys were prepared by either arc-melting or induction-melting. To insure homogeneous distribution of Sn in the alloys, the ingots were subsequently annealed in vacuum at 950°C for 72 hours. The annealed ingots were then crushed to 10 mesh in an argon glove box, followed by several hydrogen absorption/desorption cycles to activate the alloys and to obtain alloy powders of optimized surface area. The chemical composition and homogeneity of the alloys were characterized by X-ray diffractometry. X-ray data were obtained with an INEL CPS-120 powder diffractometer using Co $K\alpha$ radiation (λ = 1.7902 Å).

Pressure-composition isotherms were obtained for $LaNi_{5-x}Sn_x$ alloys by using a modified gas-manifold system described previously.[13] For the electrochemical measurements, the fine alloy powder (< 75μm) was mixed with 19°A conducive diluent, i.e., INCO nickel powder (1μm), and 5% Teflon binder. The electrodes for the cyclic lifetime studies (area: 2.54 x 2.54 cm) were fabricated by hot-pressing the mixture onto an expanded Ni screen. The electrodes for the basic electrochemical studies were fabricated by filling BAS (Bio-

Analytical Systems) disk electrodes with electrode powders of equal quantities to ensure consistent values for the electrode area (0.09 cm^2) and porosity. NiOOH electrodes from an aerospace Ni-Cd cel 1, supplied by Eagl e-Pi cher, formed the counter electrode. A three-electrode flooded cell with a 1 uggin capi llary for the Hg/l lgO reference electrode[14] was adopted for the basic electrochemical studies. For the cyclic lifetime studies, the same components were assembled in a prismatic glass cell with nylon (Pellon 2516) separator. Teflon shims were used to provide adequate compaction to the electrodes. The electrolyte contained 31 w^o/o KOH solution prepared with twice-distilled conductivity water. Electrochemical measurements (DC) were performed with an EG&G 273 Potentiostat/Galvanostat interfaced to an HIM-PC, using EG&G Corrosion Software 252. AC impedance measurements were carried out with the EG&G 273 Potentiostat and Solartron 1255 Frequency Response Anal yzer, using EG&G Impedance software 388. Cycling of the prismatic cells was carried out with an automatic battery cycler made by Arbin Corp., College Station, TX. The cycling conditions include a discharging at a constant current of 12.5 mA/cm^2 (C/2 rate) to -0.5 V vs. Hg/HgO. Charging at a constant current of 5 mA/cm^2 (C/5 rate) was performed to a charge retu n of l l 5°/0 to ensure complete charging of the metal hydride electrode.

RESULTS AND 1) ISCIJSS1ON

X-RAY DIFFRACTOMETRY

X-ray diffractometry was used to characterize the microstructure, measure the lattice parameters, and verify the phase composition of tile MH alloy. Figure 1 shows the diffraction patterns of $LaNi_{5-x}Sn_x$ alloys with different Sn compositions, x. The X-ray diffraction patterns confirmed that alloys with Sn compositions up to x = 0.5 were entirely the CaCu~-type Haucke phase. With increasing Sn concentration, the diffraction peaks shift to smaller angles (as illustrated in the insert), implying an increase in the lattice parameters. The enlargement of the unit cell upon Sn substitution is discussed below,

ISOTHERMS

To understand the hydrogen absorption and resorption characteristics of the alloys, pressure-composition isotherms were measured. Such isotherms were obtained both in the gas phase and in the electrochemical environment In addition, independent measurement of the gas-phase isotherms for several of these same alloys were made by Luo and co-workers. [15,16] Good agreement in the isotherms was found in all the cases.

Electrochemical (EC) isotherms were constructed! from the equilibrium electrode potentials at different stages of hydrogen absorption or desorption. These arc similar to coulometric titrations carried out *on* the battery electrode materials.*[7] The equilibrium electrode potentials are related to the equilibrium hydrogen pressure[18], P_{H_2}, by the Nernst equation:

$$E_o \text{ (VS. HgO/Hg)} = -0.9324-0.02.91 \log(P_{H_2}) \quad (1)$$

The EC isotherms differ slightly from the gas phase isotherms during absorption, i.e., the inflection in the pressure at the end of absorption is absent, possibly because the cell internal pressures arc limited in our cell design to about 1 atmosphere. The discharge isotherms, on the other hand, bear a greater resemblance to the gas phase isotherms. The plateau pressures calculated from EC isotherms during charge and discharge are general] y comparable to those measured by gas phase isotherms. Figure 2 shows the EC isotherms during hydrogen absorption (charge) and desorption (discharge) of $LaNi_{5-x}Sn_x$ alloys with $0.1 \leq x \leq 0.3$, along with a representative gas-phase isotherm of $LaNi_5$. The changes in the plateau pressures during absorption and resorption with a change in the Sn concentration are shown in Fig. 3. It has been noted that increasing amounts of Sn induce a lattice expansion that is linear with Sn composition.[19,20] The logarithmic decrease in plateau pressure with increasing unit cell volume seen here is consistent with the observations of Gruen et al .[2'] The hysteresis between the absorption and desorption isotherms of $LaNi_5$ is also reduced in the Sn- substituted alloys.

HYDROGEN ABSORPTION CAPACITY

The hydrogen absorption capacities of the $LaNi_{5-x}Sn_x$ alloys were measured both in the gas phase and electrochemical environments, as summarized in Fig. 4. Upon Sn substitution, the theoretical specific hydrogen absorption capacity of $LaNi_{5-x}Sn_xH_6$ decreases marginally owing to the mass of Sn atoms. The capacity measured in the gas phase is fairly close to these theoretical values. To determine the discharge capacity, all the electrodes were charged initially at 22 and 4.65 mA/cm^2 in the disc and prismatic electrode respectively, to about 400 mAh/g. This overcharge of about 20-40°/0 was used to ensure a complete hydriding of the electrodes. '] 'here is no inflection in the charge potentials at the end of charge owing to the hydrogen evolution reaction occurring at the same potentials.

After charging the disc and prismatic electrodes were discharged at 44.4 and 12.5 mA/cm^2, respectively, to -0.5 V vs. Hg/HgO. The discharge capacity improves significantly with the initial increase in Sn composition (Fig. 4). The electrochemical capacity of the binary alloy is particularly low. During its charging, significant hydrogen evolution is observed to occur on its surface, which seems to be favored over hydrogen absorption. A similar difficulty in the charging of the binary alloy has been recently reported by Wasz et al., and was overcome by operating their cel 1s at lower t emperat ures.[22] The maximum

discharge capacity measured in prismatic cells was slightly over 300 mAh/g at a discharge rate of C/2, which is an impressive value for an AB_5 alloy. For example, some of the state-of-the-art, misch metal based, AB_5 Ml I alloys evaluated at JPL showed a maximum capacity of 250-275 mAh/g. Apart from the ease in chargeability, the low plateau pressures induced by the Sn-substitution result in Ni-MH cells of low operating pressures and low self discharge.

The discharge potentials decrease with an increase in the Sn concentration. This is expected from the reduced plateau pressure with increasing Sn concentration in the alloy. The charge voltages were lower than those calculated with Eq. 1. However, the decrease in the electrochemical capacity of alloys with high Sn concentrations is significant compared to the decrease in the theoretical capacity or the hydrogen absorption capacities measured with gas-phase isotherms. From an examination of the observed mid-point potentials and the corresponding open circuit potentials obtained from the resorption plateau pressures (Fig. 5), it is clear that the discharge overpotentials tend to increase at high Sn compositions, especially for $x > 0.3$. This behavior prompted us to carry out measurements on the kinetics of electrochemical hydriding of $LaNi_{5-x}Sn_x$ alloys.

KINETICS OF HYDRIDING

DC Polarization

The kinetics of hydrogen absorption/desorption are often slowed by the alloy substituents. For example, elements forming surface films may alter the kinetics of charge transfer at, or transport of hydrogen through, the surface regions. To determine the effects of the partial substitution of Ni with Sn on the charge and discharge kinetics, DC polarization and AC impedance experiments were performed on the alloys. Micropolarization and Tafel measurements were performed on the alloys under potentiodynamic conditions at scan rates of 0.02 mV/s and 0.5 mV/s, respectively. The scan rates were so chosen to provide near-steady state. conditions with minimal changes in the state of charge of the electrode or its surface conditions.

Figure 6 shows the micropolarization curves of the $LaNi_{5-x}Sn_x$ alloys. These curves are fairly linear and spread out, owing to the difference in their equilibrium potentials. The potential of the binary alloy is less anodic (negative) than expected. This may be caused by its lower state of charge in the unsealed cell configuration. The values of the exchange currents estimated from the slopes of micropolarization curves of different MH alloys show an interesting trend (Fig. 7 and Table 1). The exchange current increases initially

upon Sn substitution from 0.77 mA for the binary alloy to 1.35 mA for the alloy with x = 0.1. This improvement in the kinetics upon Sn addition may not be unexpected, since Sn is known to have good electrocatalytic properties; for example, Pt-Sn alloys are used as electrocatal ysts in the electrochemical oxidation of methanol .[23] Further addition of Sn decreases the exchange current. Nevertheless, the kinetics of Sn substituted alloys are superior than those of the binary alloy for Sn compositions of $x \leq 0.3$. With Sn concentrations of $x \geq 0.4$, the kinetics of hydrogen absorption and resorption are slowed considerably, and are even slower than in the binary alloy. The increases in the polarization resistance at higher Sn concentrations may be caused by an incomplete activation of the MH alloy.

To determine the kinetics of absorption and desorption, Tafel polarization measurements were made on the $LaNi_{5-x}Sn_x$ alloys. Figure 8 illustrates the Tafel behavior, corrected for mass transfer, of various alloys during charge and discharge. The overpotentials at any curr ent density can be seen to decrease upon the initial substitution of Sn, but increase at (he highest Sn concentration. The cathodic Tafel plot of the binary alloy is complicated by the hydrogen evolution reaction, which occurs at the same potentials as the hydriding reaction, resulting in two distinct slopes. The simultaneous occurrence of the hydrogen evolution may result in fluctuations in the electrode potentials fi om the continual forming and bursting of hydrogen gas bubbles on the electrode surface. Such problems are

fortunately absent with Sri-substituted alloys, and the Taft] curves arc more reproducible. In any case, for the Tafel polarization experiments, the potential was scanned from extreme anodic (positive) values to the cathodic (negative) values, to avoid the uncertainties arising from hydrogen bubbles adhering to the surface of the MH electrode.

The Tafel polarization curves indicate strong mass transfer effects at high currents. The limiting currents may be related to the slow solid-state diffusion of hydrogen in the M H electrode. The limiting currents measured in a separate potentiodynamic experiment at higher positive potentials, i.e., 400 mV away from the reversible potential, are listed in Table 1. The diffusion limiting current is highest for a Sn composition of $0. \leq x \leq 0.2$ (in the range of 500 mA/g) and is reduced at high Sn compositions. Using (he measured limiting current, the Tafel plots can be corrected for the mass transfer effects by plotting the logarithm of $I/(1-I/I_{lim})$ against the elect] ode potential. The corrected Tafel plots are more linear (Fig. 8). The exchange current density and transfer coefficients for hydrogen absorpt i on and desorption were calculated from the intercept and inverse sl ope of the corrected anodic and cathodic Tafel plots, respectively. The absorption exchange current increases upon Sn substitution and shows a maximum at a Sn composition of $x = 0.2$ (Fig. 7, l'able 1). The resorption exchange current improves more significantly upon Sn substitution, but has a maximum near $x = 0.1$. Nevertheless, the kinetics of desorption continues to be better than the binary alloy for $x < 0.4$, The Tafel slopes show an

interesting trend: the slope for the absorption process decreases with increasing Sn concentration, whereas the slope for the resorption process increases (Table 1). The change in both the parameters is less marked for $x > 0.2$. It is interesting to note that the equilibrium potentials (i.e., the logarithm of the plateau pressures) vary similarly. It is known[2] that lower plateau pressures facilitate absorption, whereas higher plateau pressures are desirable for resorption. The transfer coefficients calculated from the Tafel slopes increase during absorption, with increasing Sn composition from 0.24 for x = O to 0.25,0,32, 0.34,0.35 and 0.4 for x values of 0.1, 0.2, 0.3, 0.4 and 0.S, respectively. The corresponding transfer coefficient during resorption, however, decrease with increasing Sn composition, from 0.S5 for x = O to 0.32, 0.27, 0.2.8, 0.26 and 0.26,

AC Impedance

The AC impedance data were obtained in the frequency range of 100 kHz to 5 mHz at a low AC amplitude of 2 mV. The impedance plots of $LaNi_{5-x}Sn_x$ alloy electrodes are shown in the Nyquist or Cole-Cole form in Fig. 9. As may be seen in the figure, the impedance decreases noticeably upon initial substitution of Sn but increases for $x > 0.4$. The impedance data were analyzed using a generalized equivalent circuit adopted for the Ml 1 electrode.[24] The capacitive components are modeled as constant-phase elements (CPE) to describe the depressed nature of the semi-circles.[25] R_1 is ascribed to the

electrolyte resistance between the MH electrode and the reference electrode. The semi-circle in the high frequency region, represented by R_2 and Q_2, results from the contact resistance between the current collector and the teflon-bonded electrode. The parameters R_3 and Q_3 are attributed to the contact resistance and the capacitance between the particles of the plastic-bonded metal hydride powder. The semi-circle in the low frequency region, represented by R_4 and Q_4 is attributed to the reaction (charge transfer) resistance and the double-layer capacitance, respectively. The diffusional impedance, W_4, is the Warburg impedance, which is a parallel and/or series combination of diffusional resistance and pseudo-capacitance. The observed impedance patterns of the M H electrodes (Fig. 9) are simplified by the absence of a diffusional component. The other parameters in the equivalent circuit were calculated by a non-linear least squares fit using the Boukamp method.[26]

The exchange current calculated from the charge transfer resistance decreases initially upon the substitution of Sn but increases for Sn compositions $x \geq 0.4$ (Table 1). The trend is similar to that observed in the DC polarization experiments. It is thus clear that the kinetics of hydriding improves markedly upon Sn substitution in $LaNi_{5-x}Sn_x$, at least for $x \leq 0.3$. I Iigher amounts of Sn seem to cause sluggish kinetics for hydrogen absorption and resorption. This behavior is currently being studied in more detail.

CYCLIC LIFETIME

Finally, the performance of the MH alloys during charge-discharge cycling was evaluated in 250 mAh, negative-limited, prismatic, laboratory test cells. Although sealed cells are typically positive-limited in order to utilize an overcharge mechanism, the present cells were designed in the negative-limited configuration (with a deficit of MH) to investigate the life-limiting mechanisms of the MH electrode.. The cyclic lifetimes under these accelerated test conditions are expected to be shorter than in sealed commercial cells, but these tests should be appropriate for comparative evaluation of cyclic lifetimes of different metal hydride electrode materials.

The cyclic lifetime of cells containing $LaNi_{5-x}Sn_x$ metal hydride alloys are presented in Fig. 10. The cyclic lifetime data were smoothed by appropriate polynomial trend lines to eliminate instrument induced variations. Figure 10 shows that the initial capacity increases with an increase in the Sn composition, We attribute the lower capacities of the Sn-poor alloys to their high plateau pressures, which were around 1 atm. Since our cells operated only slightly above 1 atm., incomplete charging is expected for the alloys with $x < 0.2$. However, the initial capacity declines again at high Sn compositions, i e., $x \geq 0.4$, While suppressed hydrogen absorption/resorption kinetics could also be responsible for this trend at high Sn concentrations, we attribute this effect to the loss of intrinsic

capacity of the alloy, incomplete activation, and the low resorption pressures of the alloys. A Sn composition of $0.2 \leq x \leq 0.3$ provides the highest initial capacity of approximately 300 mAh/g.

Each cell was subjected to 200 charge-discharge cycles. The retention of capacity was found to improve with increasing Sn composition. After 100 charge-discharge cycles, alloys with $x = 0.25$ or 0.3 exhibit capacities in excess of 200 mAh/g, an impressive number when compared to the state of art $MmNi_{3.5}Co_{0.8}Mn_{0.4}Al_{0.3}$ MH alloys evaluated at JPL[27] (Fig. 10, curve 8). It is interesting to note that alloys with high Sn compositions ($x \geq 0.4$) show long activation cycles; with these compositions the maximum capacity is achieved only after 30 cycles. The lifetime capacity in cells with $x \geq 0.4$ exceeds that of cells with $0.2 \leq x \leq 0.3$, as evidenced by the lifetime curves after 150 cycles.

CONCLUSIONS

The substitution of small amounts of Sn for Ni in $LaNi_5$ improves many characteristics of the metal hydride anode in alkaline rechargeable cells. Specifically, the chargeability is improved owing to reduced absorption plateau pressures. The hydrogen absorption capacity of the $LaNi_{5-x}Sn_x$ alloys approaches 300 mAh/g, an impressive number for an AB_5 formulation. The kinetics of hydrogen absorption and desorption are improved

markedly compared to the binary alloy, although at high Sn concentrations the improvement is less evident, possibly resulting from incomplete activation. 'I'he capacity retent i on during charge-discharge cycling is significantly enhanced such that the cyclic lifetime of Sn substituted alloys is comparable to some multi-component, misch-metal based alloys. Tin compositions in the range of $0.2 \leq x \leq 0.3$ appear to be optimal for high capacities, long cyclic lifetime and improved kinetics. W c suggest that higher Sn compositions ($0.4 \leq x \leq 0.5$) may be favored for high temperature applications. The simple alloy chemistry and absence of Co in these alloys gives them an economic advantage over the $Mm(NiCoAlMn)_5$ alloys now being produced commercially.

ACKNOWLEDGMENTS

This work was carried out at the Jet Propulsion Laboratory under contract with the National Aeronautics and Space Administration and at the California Institute of Technology under funding by the DOE grant DE-FG03-94ER14493. We thank I.,. A. Wade of JPL for providing samples of several alloys and Prof. T.B. Flanagan of Univ. of Vermont, for supplying detailed results of their isotherm measurements.

REFERENCES

1. J. J. G. Willems, *Philips J. Res.*, 39 (Suppl. 1), 1 (1984); J. J. G. Willems and K. H. J. Buschow, *J. Less Common Metals*, 129, 13 (198'/),

2. T. Sakai, K. Muta, H. Miyamura, N. Kuriyama and H. Ishikawa, *Proc. Symp. Hydrogen Storage Materials: Batteries and Electrochemistry*, ECS Proc. Vol. 92-5, p.59 (1992); T. Sakai, H. Yoshinaga, H. Mi yamura and H. Ishikawa, *J. Alloys and Compounds*, 180,37(] 992).

3. S. R. Ovshinsky, M. A. Fetcenko and J. Ross, *Science*, 260, 176 (1993); M. A. Fetcenko, S. Venkatesan and S. R. Ovshinsky, *Proc. Symp. Hydrogen Storage Materials : Batteries and Electrochemistry*, ECS Proc. Vol. 92-5, p. 141 (1 992); M. A. Fetcenko, S. Venkatesan, K. C. Hong and B. Reichman, *Power Sources*, Vol. 12, p. 411 (1988).

4. T. Sakai, K. Oguru, H, Miyamura, N. Kuriyama, A. Kato and H. Ishikawa, *J. Less-Common Mets/.v*, 161, 193 (1990).

5, T. Sakai, H. Miyamura, N. Kuriyama, A. Kato and K. Oguru *J. Less-common Metals, 159*, 127 (1 990).

6. T. Sakai, H. Miyamura, N. Kuriyama, A. Kate, K. Oguru and H. Ishikawa, *J. Electrochem.* Sot., 137, 795(1 990).

7.3'. Sakai, T. Hazama, H. Miyamura, N. Kuriyama, A. Kato and H. Ishikawa, *J. Less-Common Metals*, 172-174, 1175 (1991).

8. N. Furukawa et al (Sanyo Electric Co.), *Proc. IBA Meeting*, Seattle, WA, Oct. 12-13 (1990).

9. 1. Matsumoto and A. Ohta (Matsushita, Japan), *Proc. IBA Meeting*, Seattle, WA, Ott 12-13 (1990).

10 B. V. Ratnakumar, G. Halpert, C. Witham and B Fultz, *J. Electrochemical Sot.*, 141, 189 (1 994).

11 B. V.. Ratnakumar, S. Surampudi, S. Di Stefano, G. Halpert, C. Witham, A. Hightower and B. Fultz, *Proc. ECS Symp. Hydrogen Batteries*, Miami Beach, FL. 94-27, 57 (1994),

12. A. Anani, A. Visintin, K. Petrov and S. Srinivasan, *J. Power Sources*, 47,261 (1994).

13. R. C. Bowman , Jr., C. H. Luo, C. C. Ahn, C. K. Witham and B. Fultz, J. *Alloy Conlpomds>217,* 185 (1 995).

14.11. V. Ratnakumar, S. Di Stefano, S. Surampudi and G. Halpert, *J. Electrochem. Sot.,* (in press).

15. S. Luo, W. Luo, J. D. Clewley, T. B. Flanagan and R. C. Bowman, *J. Alloy Compounds* (In press).

16. S. Luo, W. Luo, J. D. Clewley, T. B. Flanagan and L. A. Wade, *J. Alloy Compounds* (In press).

17. For example, A. Anani and R. A. Huggins, *J. Power Sources,* 38,363 (1992).

18. C. Jordy, A. Percheron-Guegan, J. Bouet, P. Sanchez, C. Chanson and J. Leonardi, *J. Less Common Metals,* 172-174, 1236 (1991).

19. M. Mendelsohn, D. Gruen, A. Dwight, *Inorg. Chem.* 18, 3343 (1979).

20. J. S. Cantrell, T. A. Beiter and R. C. Bowman, Jr., J. *Alloys and Compounds, 207/208, 372 (1994).*

21.11. N. Gruen, M. H. Mendelssohn and A, E. Dwight, *J. Less Common Met.*, 63, 193 (1979).

22. M. Wasz, R. B. Schwarz, S. Srinivasan and M. P. Sridhar Kumar, Proc. MRS Spring Meeting, San Francisco, CA, April)7-20 (1995).

23. M. M. P. Janssen and J. Moolhuysen, *Electrochim. Acta., 21,* 861 and *869 (1976).*

24. N. Kuriyama, T. Sakai, H. Miyamura, I. Uehara and H. Ishikawa, *J. Alloys and Compounds, 192,* 161 *(1 993).*

25. J. Ross McRonald, *Impedance Spectroscopy*, John Wiley & Sons, NY (1 *987).*

26, B. A. Boukamp, *Solid State Ionics*, *20,31* (19S6)

27.11. V. Ratnakumar, S. Surampudi, S. Di Stefano and (;. 1 lalpert, *Proc. 36th Power Sources Conf.*, Cherry Hill, NJ, June 6-9(1994).

FIGURE CAPTIONS

Fig. 1 : X-ray diffraction patterns of $LaNi_{5-x}Sn_x$ alloys. The insert shows the diffraction peaks shifting to smaller angles with increasing Sn composition.

Fig. 2: P-c-T isotherms of $LaNi_{5-x}Sn_x$ alloys: Electrochemical (○, ● x = 0.3; O, ♦ x = 0.2; □,■ x== O. 1; open - charge, closed - discharge), and gas-phase (-).

Fig. 3: Variation with the Sn composition, x, in $LaNi_{5-x}Sn_x$ alloys of unit cell volume (.) and plateau pressure (■) for 300 K absorption.

Fig. 4: Hydrogen absorption capacity of $LaNi_{5-x}Sn_x$ alloys measured with Sieverts' apparatus, prismatic cell electrode and BAS electrode, and theoretical capacity for H/M ratio of 1:1.

Fig. S: Variation of mid-point discharge potentials and the corresponding calculated reversible potentials from the resorption plateau pressures.

Fig. 6: linear polarization curves of $LaNi_{5-x}Sn_x$ alloys

Fig. 7: Variation of the exchange current density from measurements by DC micropolarization (■), AC Impedance (x), Anodic Tafel polarization (.) and Cathodic Tafel polarization (---).

Fig. 8: Tafel polarization curves with mass transfer corrections of $LaNi_{5-x}Sn_x$ alloys.

Fig, 9: Electrochemical Impedance Spectroscopy (EIS) curves of $LaNi_{5-x}Sn_x$.

Fig. 10: Cyclic lifetime behavior of $LaNi_{5-x}Sn_x$ alloys with comparison to the best Misch-metal based, multi-component alloy evaluated at JPL (ref. 27).

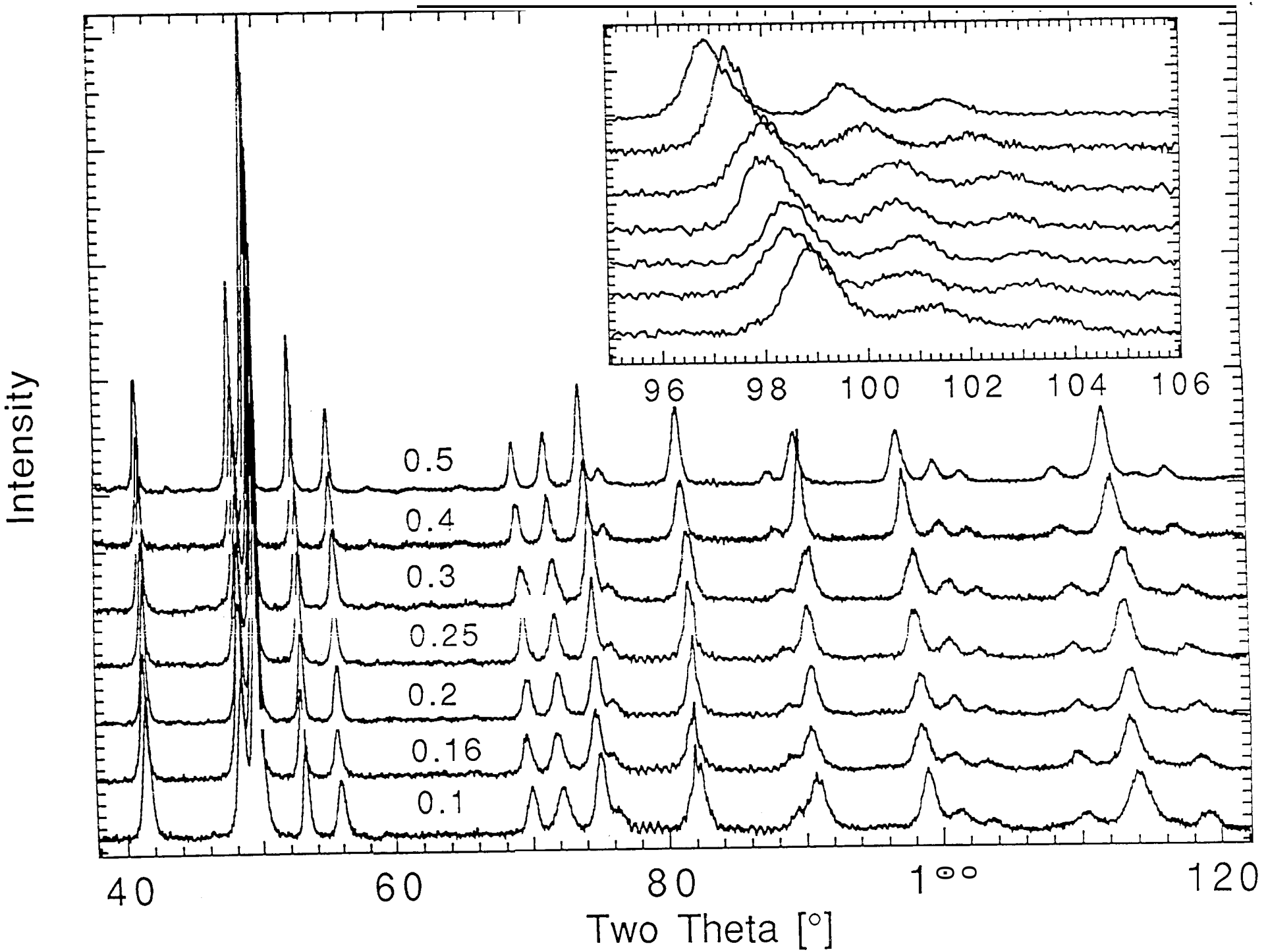
Intensity
0.5
0.4
0.3
0.25
0.2
0.16
0.1
96
98
100
102
104
106
40
60
80
1oo
120
Two Theta [°]

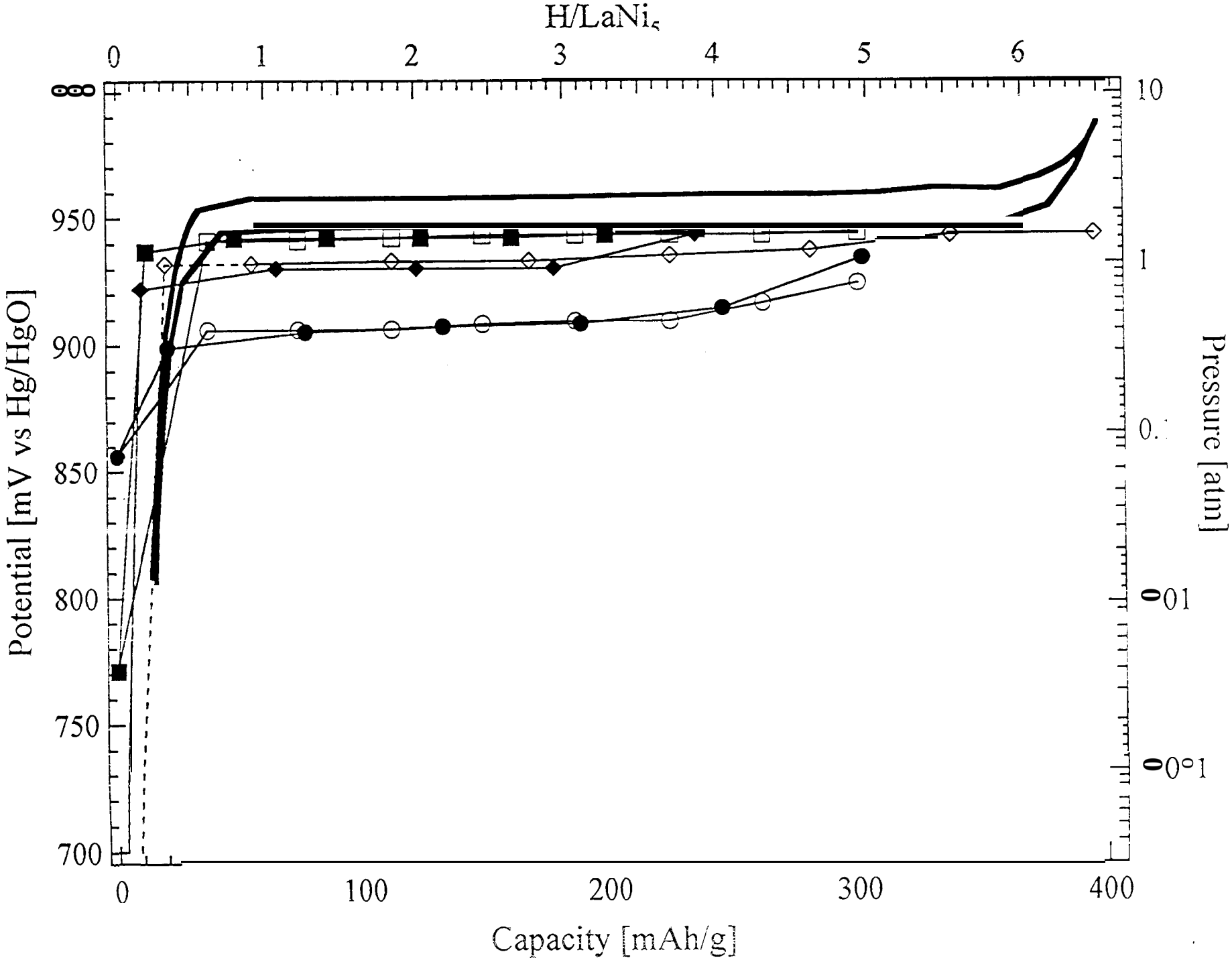
H/LaNi5
0
1
2
3
4
5
6
Potential [mV vs Hg/HgO]
950
900
850
800
750
700
10
1
0.1
0.01
Pressure [atm]
0
100
200
300
400
Capacity [mAh/g]

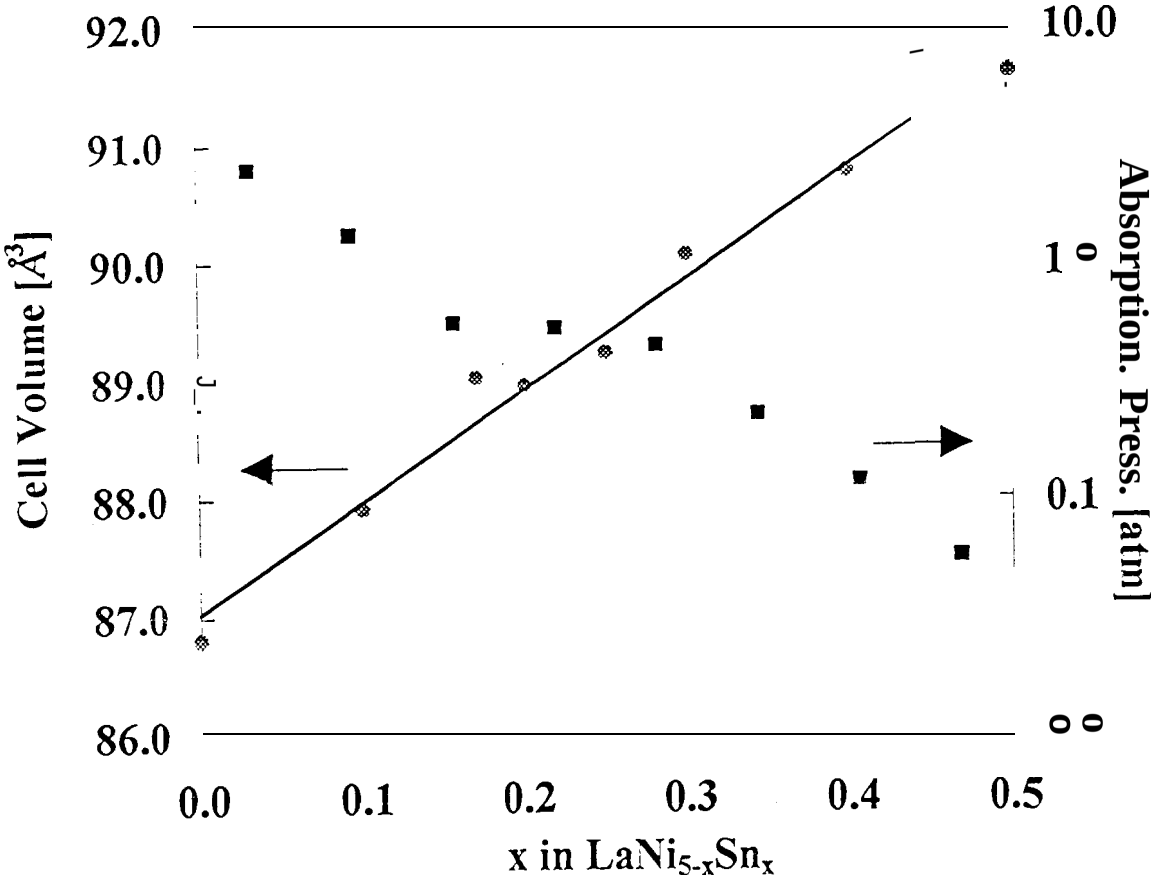

B. V. Ratnakumar, et al.

Figure 3

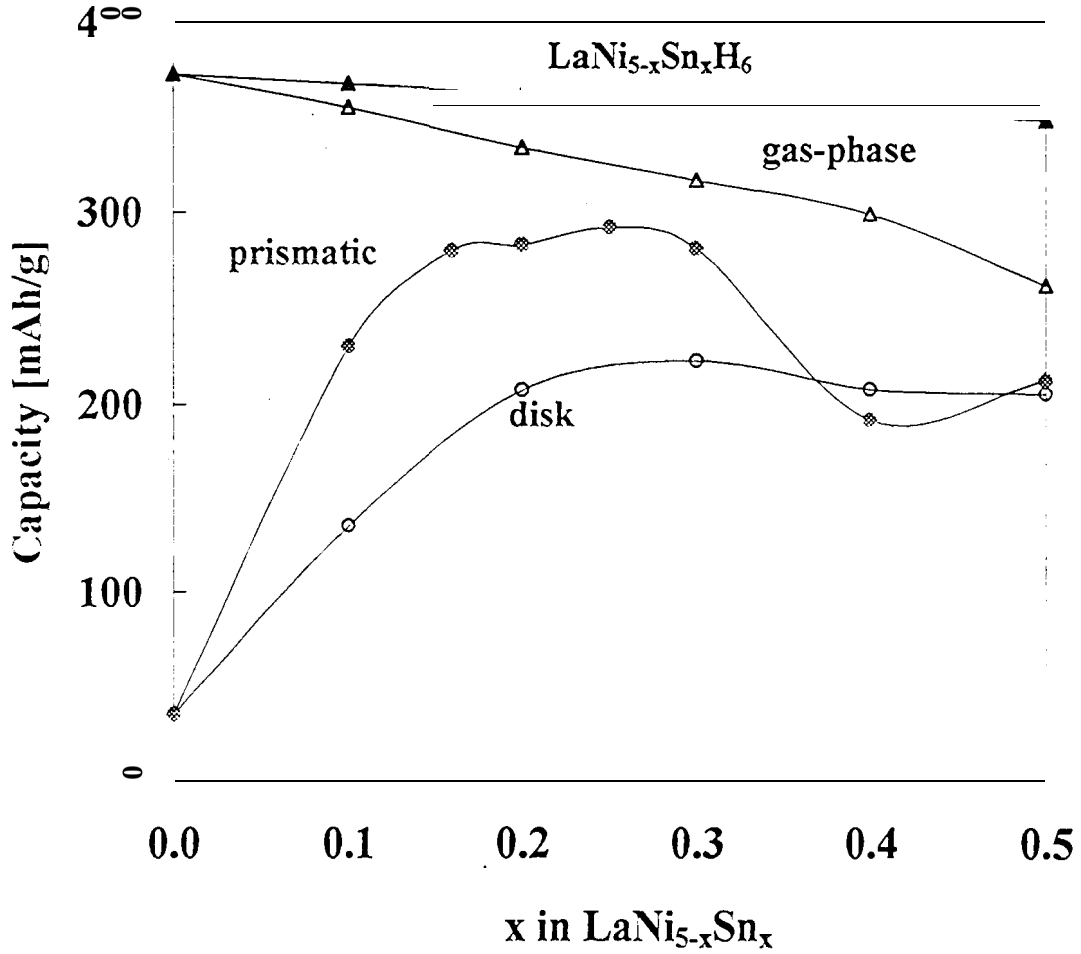

Ratnakumar, et al.

Figure 4

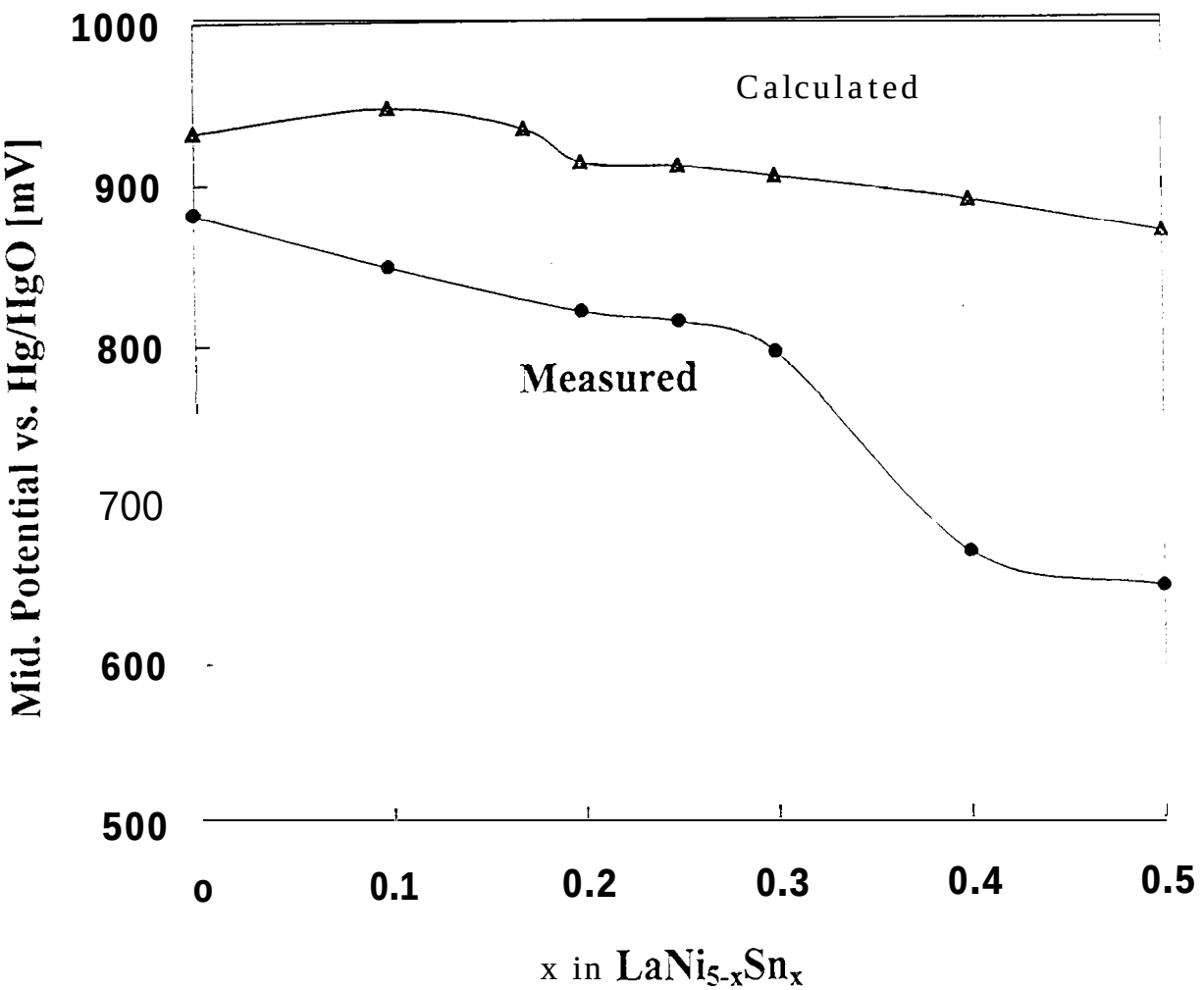

B. V. Ratnakumar, et al.

Figure 5

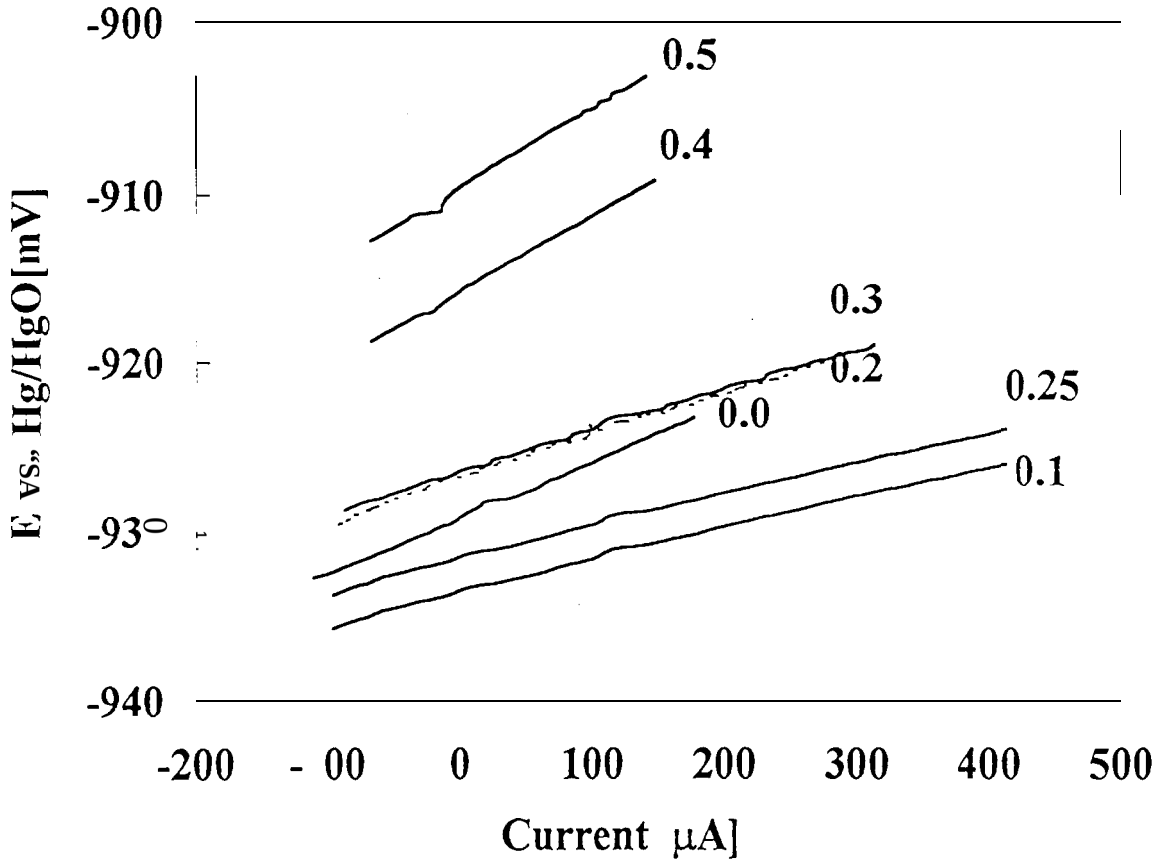

B. Ratnakumar, et al.

Figure 6

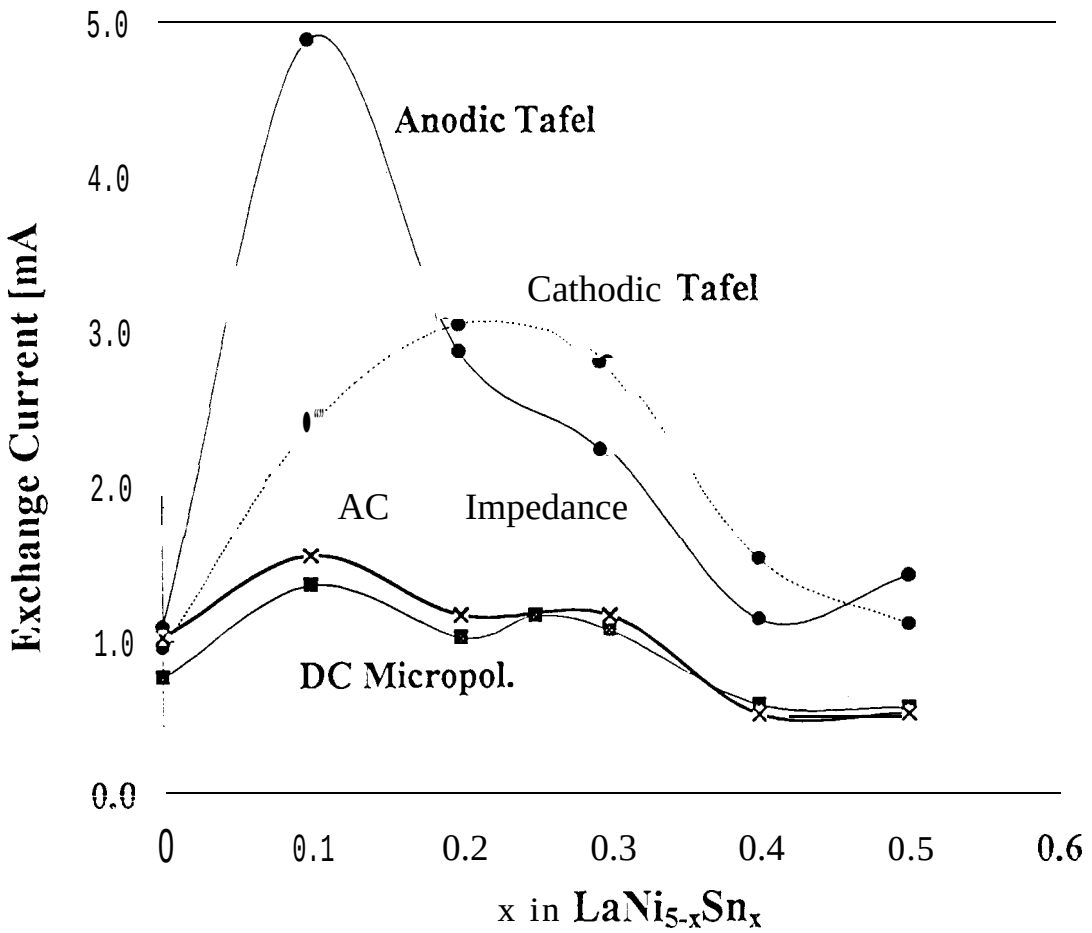

B. V. Ratnakumar, et al.

Figure'7

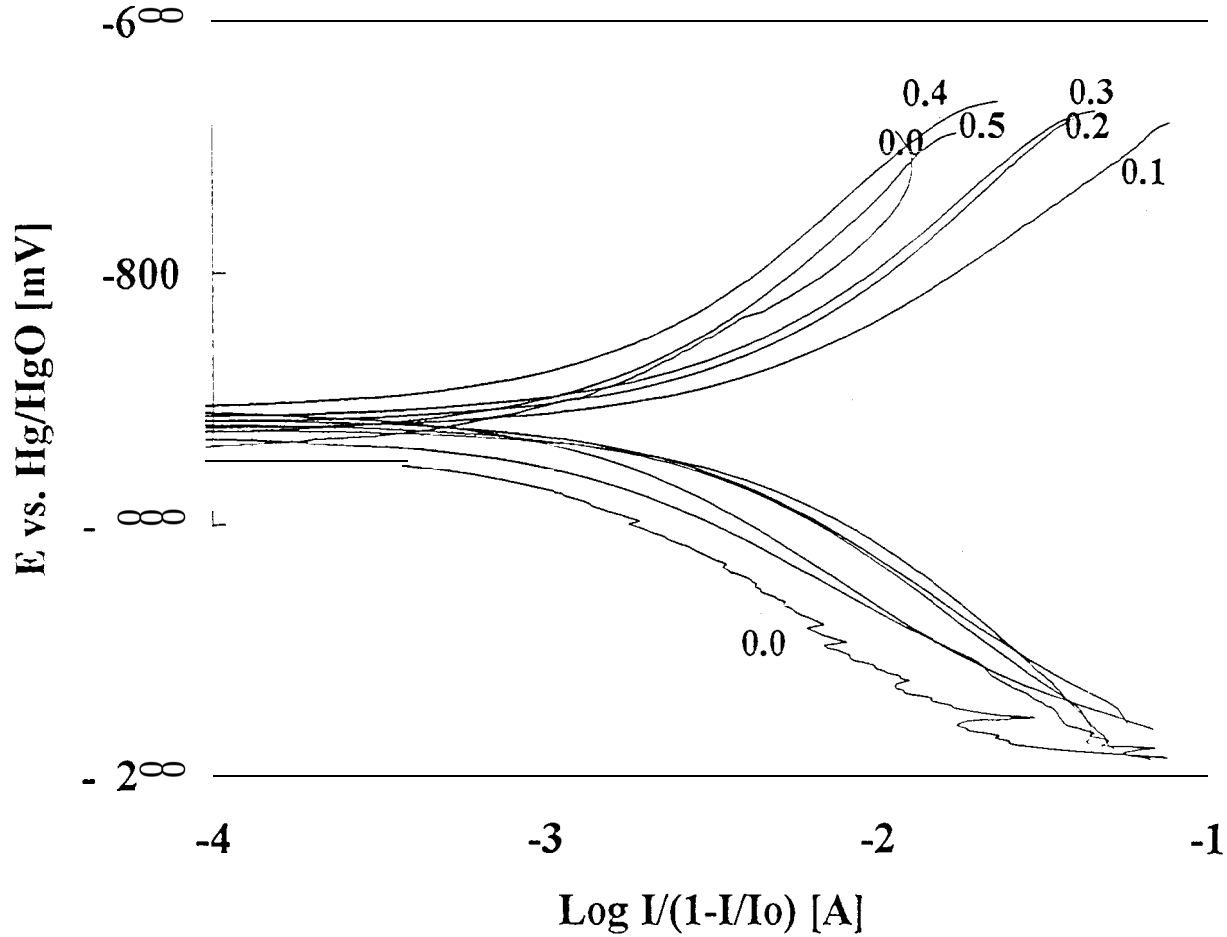

B. V Ratnakumar, et al.

Figure 8

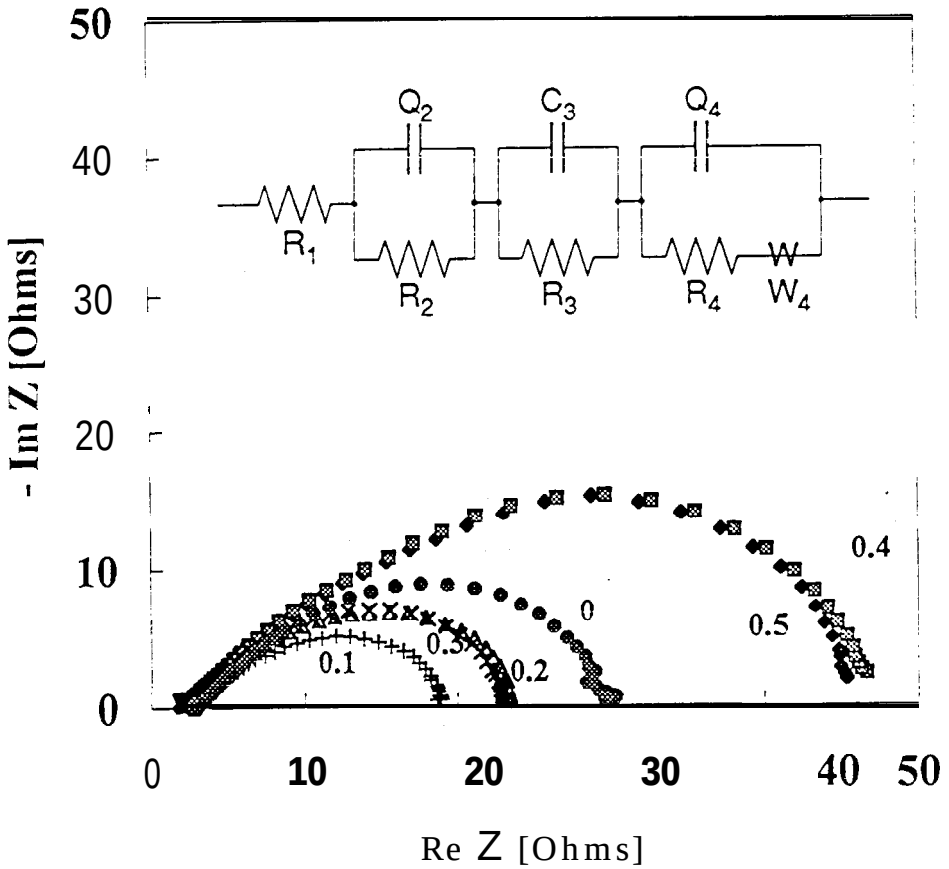
50
40
30
20
10
0
- Im Z [Ohms]
0
10
20
30
40
50
Re Z [Ohms]
Q2
C3
Q4
R1
R2
R3
R4
W
W4
0.4
0
0.5
0.3
0.1
0.2

Figure 9

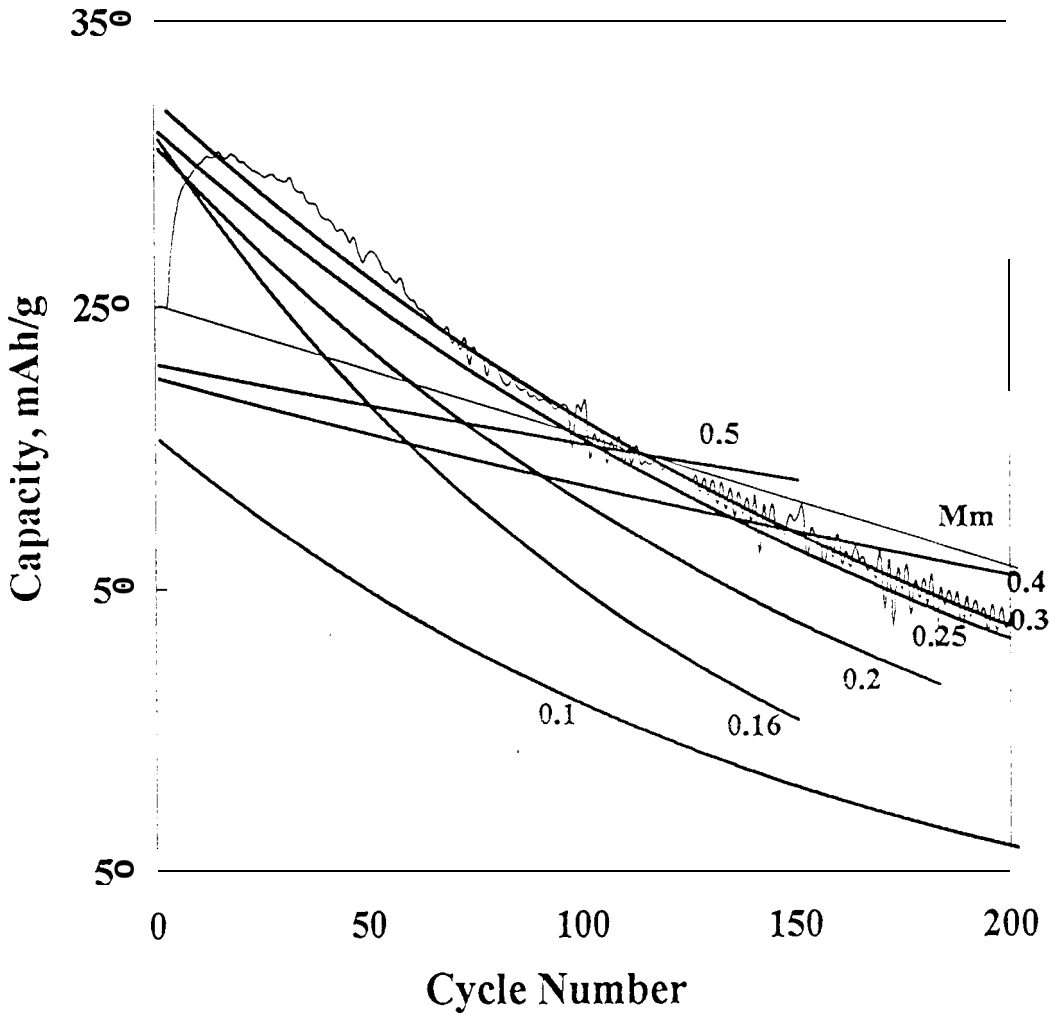

B. V. ak et al.

Figure 10